THE JOURNAL OF PHYSICAL CHEMISTRY B

ARTICLE

pubs.acs.org/JPCB

# Effect of $SO_2$ on the Transport Properties of an Imidazolium Ionic Liquid and Its Lithium Solution

Marcelo J. Monteiro,[†] Rômulo A. Ando,[†] Leonardo J. A. Siqueira,[‡] Fernanda F. Camilo,[‡] Paulo S. Santos,[†] Mauro C. C. Ribeiro,[†] and Roberto M. Torresi*[,†]

[†]Instituto de Química, Departamento de Química Fundamental, Universidade de São Paulo, C.P. 26077, CEP 05513-970, São Paulo, SP, Brazil

[‡]Laboratório de Materiais Híbridos, Departamento de Ciências Exatas e da Terra, Instituto de Ciências Ambientais, Químicas e Farmacêuticas, Universidade Federal de São Paulo, Rua Napoleão de Barros, 598, CEP 04024-002, São Paulo, SP, Brazil

Supporting Information

**ABSTRACT:** Transport coefficients have been measured as a function of the concentration of sulfur dioxide, $SO_2$, dissolved in 1-butyl-2,3-dimethylimidazolium bis(trifluoromethylsulfonyl)-imide, [BMMI][$Tf_2N$], as well as in its lithium salt solution, Li[$Tf_2N$]. The $SO_2$ reduces viscosity and density and increases conductivity and diffusion coefficients in both the neat [BMMI][$Tf_2N$] and the [BMMI][$Tf_2N$]−Li[$Tf_2N$] solution. The conductivity enhancement is not assigned to a simple viscosity effect; the weakening of ionic interactions upon $SO_2$ addition also plays a role. Microscopic details of the $SO_2$ effect were unraveled using Raman spectroscopy and molecular dynamics (MD) simulations. The Raman spectra suggest that the $Li^+$−[$Tf_2N$] interaction is barely affected by $SO_2$, and the $SO_2$−[$Tf_2N$] interaction is weaker than previously observed in an investigation of an ionic liquid containing the bromide anion. Transport coefficients calculated by MD simulations show the same trend as the experimental data with respect to $SO_2$ content. The MD simulations provide structural information on $SO_2$ molecules around [$Tf_2N$], in particular the interaction of the sulfur atom of $SO_2$ with oxygen and fluorine atoms of the anion. The $SO_2$−[BMMI] interaction is also important because the [BMMI] cations with above-average mobility have a larger number of nearest-neighbor $SO_2$ molecules.

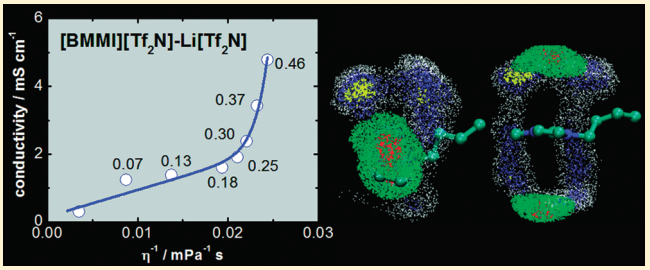


## INTRODUCTION

Room-temperature ionic liquids (ILs) are one of the most promising substitutes for conventional organic solvents by virtue of their high chemical and thermal stabilities, as well as their near-zero vapor pressures.[1,2] Several possibilities for using ILs as an alternative medium for many chemical processes, along with their unique physicochemical properties, suggest different areas of application for ILs, including the industrial,[3] environmental,[4−7] engineering,[8,9] nanomaterials,[10−12] and high-tech sectors.[13] Despite the exponential increase in publications on ILs at a more fundamental level, the understanding of the physicochemical properties of ILs is still a major point of discussion, as are several experimental and theoretical approaches being proposed to explain how their structures account for their low melting temperatures.[14−16]

Beyond the microscopic understanding of their fluidity at ambient temperatures, the next step is controlling the factors that determine properties such as density, viscosity, diffusion coefficients, conductivity, etc. The numerous ways to chemically modify and combine different cations and anions open up the exciting possibility of tuning their properties to the desired application. As an example of the sensitive properties of ILs, Fumino et al.[17] showed that a simple substitution of a methyl group by a hydrogen atom on the imidazolium ring causes the appearance of hydrogen bonds between ions. The hydrogen bonds break the charge symmetry network and thus fluidize the IL. Despite the interesting discussion opened by Lassègues et al. about the IR assignment of the $\nu$(C−H) vibrational mode,[18−20] the main conclusion of Fumino et al. is that the properties of ILs can be altered by the proper adjustment of the ratio between the Coulomb and van der Waals interactions.[17]

Another way to modify the physicochemical properties is to dissolve molecular or ionic species in ILs. In previous reports, we showed that $SO_2$ fluidizes 1-butyl-3-methylimidazolium bromide, [BMI]Br, resulting in drastic changes in its viscosity, diffusion coefficients, and ionic conductivity.[21,22] In comparison to the pure [BMI]Br molten phase, an increase of up to 3 orders of magnitude in the diffusion coefficients and conductivity in the presence of $SO_2$ was observed.[21] These drastic changes were attributed to the shielding effect on Coulomb interactions between ions by the specific $SO_2$−$Br^-$ interaction.[22] Much experimental and

**Received:** May 17, 2011
**Revised:** June 30, 2011
**Published:** July 05, 2011

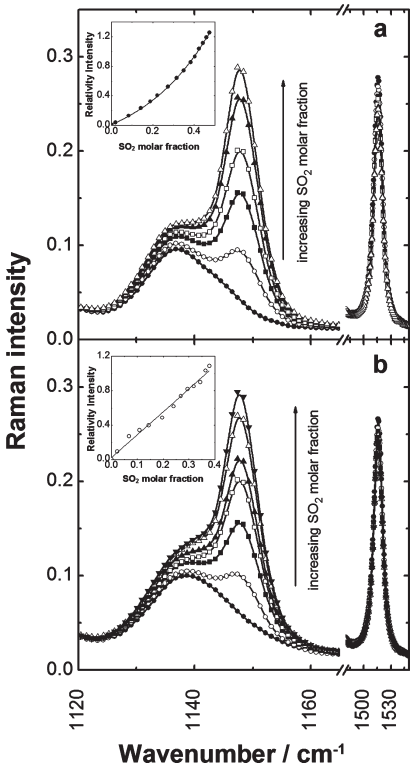


**Figure 1.** Dependence of Raman spectra on the $SO_2$ molar fraction: (a) [BMMI][$Tf_2N$], (b) [BMMI][$Tf_2N$]−Li[$Tf_2N$], at $x_{LiTf_2N}$ = 0.24. Insets show $I_{SO_2}/I_{BMMI}$ vs $x_{SO_2}$, where the ratio of Raman intensities corresponds to the $SO_2$ normal mode at 1148 $cm^{-1}$, and to the [BMMI] normal mode at 1516 $cm^{-1}$.

theoretical evidence is available concerning the nature of such interactions, for instance, the shift to a lower wavenumber of the symmetric stretching mode observed in the Raman spectrum of $SO_2$, $\nu_s(SO_2)$.[21] A question arises about whether these changes in IL properties are specifically dependent on the $SO_2$−anion interaction. We have also investigated the effect of adding the strongly polarizing lithium cation on the transport coefficients of the ionic liquid 1-butyl-2,3-dimethylimidazolium bis(trifluoromethylsulfonyl)imide, [BMMI][$Tf_2N$].[23] In this case, adding $Li^+$ increases the viscosity and decreases the conductivity, and molecular dynamics (MD) simulations showed that the strong $Li^+$−[$Tf_2N$] interaction promotes significant changes in the IL structure.

In this work, we address the changes in the physicochemical properties of [BMMI][$Tf_2N$] and [BMMI][$Tf_2N$]−Li[$Tf_2N$] solutions upon the addition of $SO_2$. The influence of $SO_2$ on the transport properties of the [BMMI][$Tf_2N$]−Li[$Tf_2N$] solution is interesting because of the detrimental effects of lithium cations on the conductivity and viscosity of ILs. Therefore, an improvement in lithium transport would be achieved after dissolving $SO_2$ in an IL. However, a less specific interaction between $SO_2$ and the delocalized [$Tf_2N$] anion is expected compared to the interactions in the previous study of the bromide anion.[21] Thus, MD simulations have been performed to provide insights into how $SO_2$ modifies the structure and dynamics of the ionic liquid [BMMI][$Tf_2N$].

## EXPERIMENTAL SECTION

The IL [BMMI][$Tf_2N$] was synthesized and purified as previously described.[24] The water content of the ILs was measured using the standard Karl-Fischer method and was determined to be below 100 ppm. Gaseous $SO_2$ (White-Martins, 99.95%) was used with no further purification and dried by passing the gas through pure sulfuric acid. The samples were handled in dry conditions inside a glovebox (Labmaster 130) under an argon atmosphere. The pure $SO_2$ was bubbled into a known mass of [BMMI][$Tf_2N$] until saturation ($x_{SO_2} \cong 0.5$), and a lower molar fraction was obtained after bubbling argon and controlling the total mass using an analytical balance with an accuracy of 0.1 mg.

To guarantee the same $SO_2$ content in different measurements, we constructed an analytical curve relating $x_{SO_2}$ and the Raman intensity ratio $I_{SO_2}/I_{BMMI}$ of the band at 1148 $cm^{-1}$, assigned to $\nu_s(SO_2)$, and the intense band at 1516 $cm^{-1}$ of the [BMMI] cation (see Figure 1 below). The Raman spectra were recorded in a Bruker RFS 100 system using the 1064 nm line of a Nd/YAG laser, typically with 300 mW of output power and a spectral resolution of 1.0 $cm^{-1}$. The same $I_{SO_2}/I_{BMMI}$ ratio was observed before and after measurements of transport coefficients; i.e., no significant loss of $SO_2$ occurred during the experiments.

Viscosity measurements were performed in an Anton Paar Stabinger SVM 3000, and ionic conductivity was measured with the impedance method with an Autolab PGSTAT 30 (Eco Chemie) within the frequency range 0.1−100 kHz at 36 °C inside the glovebox. Diffusion coefficients were measured by pulsed-gradient spin−echo nuclear magnetic resonance (PGSE-NMR) in a Varian INOVA 300 MHz spectrometer equipped with a 5 mm indirect detection probe (22 G $cm^{-1}$ max), calibrated with water, $D = 2.299 \times 10^{-9}$ $m^2$ $s^{-1}$ at 298 K. A stimulated spin−echo pulse sequence, i.e., 90°−$\tau_1$−90°−$\tau_2$−90°−$\tau_1$−acquisition, that incorporated a gradient pulse in each $\tau_1$ period was used. The echo attenuation was fit by the following equation

$$\ln\left(\frac{I}{I_0}\right) = -\gamma^2 g^2 \delta^2 D\left(\Delta - \frac{\delta}{3}\right) \quad (1)$$

where $g$ is the gradient strength, $I_0$ is the echo amplitude when $g$ tends to zero, $\gamma$ is the gyromagnetic ratio, $\delta$ is the duration of the gradient pulse, and $\Delta$ is the time between gradient pulses. Samples were kept in sealed NMR tubes to maintain the $SO_2$ concentration.

## COMPUTATIONAL DETAILS

The MD simulations were performed with a pairwise nonpolarizable model in which the potential energy function includes intermolecular Lennard-Jones and Coulombic interactions, as well as intramolecular interactions for bond stretching, $r$, angle bending, $\theta$, and torsion of dihedral angles, $\psi$

$$V_{total} = \sum_{\substack{i,j \\ i<j}} \left\{ 4\varepsilon_{ij}\left[\left(\frac{\sigma_{ij}}{r_{ij}}\right)^{12} - \left(\frac{\sigma_{ij}}{r_{ij}}\right)^{6}\right] + \frac{q_i q_j}{r_{ij}} \right\} + \sum_{bonds} k_b(r - r_{eq})^2 + \sum_{angles} k_\theta(\theta - \theta_{eq})^2 + \sum_{dihedrals} k_\psi[1 + \cos(n\psi - \delta)] \quad (2)$$

where $r_{ij}$ is the distance between atoms $i$ and $j$ of different ions, $r_{eq}$ and $\theta_{eq}$ are equilibrium bond lengths and angles, and $n$ and $\delta$ are

dihedral-angle parameters. The inter- and intramolecular parameters for [BMMI][$Tf_2N$] and $SO_2$ were the same used in previous MD simulations.[21−23,25] The cross-term parameters are given by the usual combining rules: $\varepsilon_{ij} = (\varepsilon_i\varepsilon_j)^{1/2}$ and $\sigma_{ij} = {}^1/_2(\sigma_i + \sigma_j)$. A united-atom model was used for the [BMMI] cation, in which hydrogen atoms are not considered in $CH_3$, $CH_2$, and CH groups.

The MD simulations of [BMMI][$Tf_2N$]−$SO_2$ were performed in a cubic box containing 200 $\mu_B MI^+$ cations, 200 TFSI anions, and 20, 50, 100, and 200 $SO_2$ molecules to obtain molar ratios of 0.1, 0.25, 0.5, and 1.0, respectively. To compare [BMMI][$Tf_2N$]−$SO_2$ and pure [BMMI][$Tf_2N$], MD simulations were also performed for a system containing 200 pairs of [BMMI][$Tf_2N$]. The simulation of [BMMI][$Tf_2N$]−$SO_2$ was performed at 330 K for a direct comparison with previously reported experimental properties.[23] Simulations of pure [BMMI][$Tf_2N$] were also performed at 330 K. Initial configurations were generated with the help of the Packmol package.[26] During the first 500 ps of the equilibration run, the box size was allowed to change to maintain a density in reasonable agreement with the experiment at an average pressure of 1 bar. At the equilibrium density, an additional 500 ps of equilibration runs were performed for both systems. In all simulations, a time step of 3.0 fs was used, and production runs were 6.0 ns long. Temperature and pressure were controlled using the method described by Berendsen et al.,[27] which involves weak coupling to a bath. Coulombic interactions were handled by the Ewald sum method.[28] Further computational details can be found in previous publications.[21−23]

## RESULTS AND DISCUSSION

**Raman Spectra.** Figure 1 shows the Raman spectra of [BMMI][$Tf_2N$] and [BMMI][$Tf_2N$]−Li[$Tf_2N$] solutions with increasing $x_{SO_2}$, and insets show the ratio $I_{SO_2}/I_{BMMI}$ vs $x_{SO_2}$. (Full Raman spectra are shown in Figure 1s and 2s in the Supporting Information.) The $SO_2$ symmetric stretching mode, $\nu_s(SO_2)$, is the Raman band at 1148 $cm^{-1}$ that grows with $x_{SO_2}$, and the relatively weak and broad band observed at approximately 1138 $cm^{-1}$ is assigned to the [$Tf_2N$] anion. The band at 1516 $cm^{-1}$ can be assigned to a $NC(CH_3)NCCH_3$ stretching mode of the [BMMI] cation.[29] There is a smooth dependence of $I_{SO_2}/I_{BMMI}$ on $x_{SO_2}$, which validates the method of checking the $SO_2$ content in the investigated ionic liquids by Raman spectroscopy. Interestingly, the wavenumber of the $\nu_s(SO_2)$ mode does not change with $x_{SO_2}$, and this value of 1148 $cm^{-1}$ is the same as $SO_2$ in nonpolar solvents, such as carbon tetrachloride and *n*-hexane. This finding indicates a much weaker $SO_2$−[$Tf_2N$] interaction in comparison with a $SO_2$−$Br^-$ interaction, in which the wavenumber shifts with the $SO_2$ content; a maximum value $\nu_s(SO_2) \sim 1138$ $cm^{-1}$ was observed for $SO_2$ saturated in [BMI]Br. Thus, the upward shift of $\nu_s(SO_2)$ observed in [BMMI][$Tf_2N$]−$SO_2$ can be rationalized by the much more delocalized electronic structure of the [$Tf_2N$] anion, which consequently represents a much weaker Lewis base in comparison to halides. Furthermore, it should be mentioned that the doublet of bands at 740 and 747 $cm^{-1}$ in the [BMMI]-[$Tf_2N$]−Li[$Tf_2N$] solution (see Figure 9 in ref 30), which are due to [$Tf_2N$] anion and coordinated [$Tf_2N$]−$Li^+$, respectively, was observed here and it was not altered upon addition of $SO_2$ (Figure 3s in the Supporting Information). Therefore, the strong [$Tf_2N$]−$Li^+$ interaction is not significantly perturbed by $SO_2$ molecules.

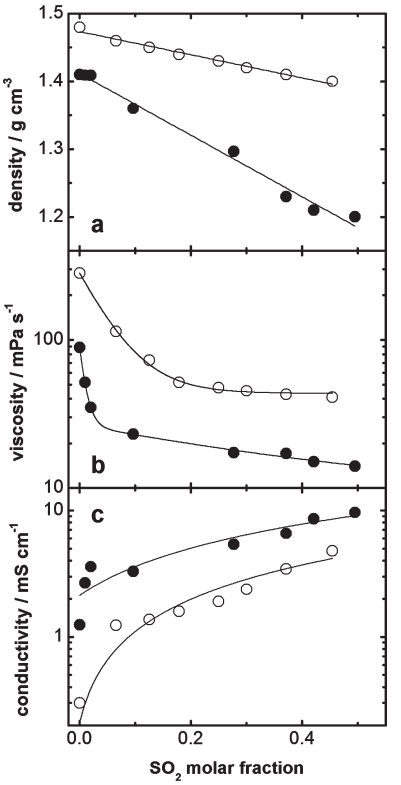


**Figure 2.** (a) Density, (b) viscosity, and (c) conductivity as functions of the $SO_2$ molar fraction: (●) [BMMI][$Tf_2N$], (○) [BMMI][$Tf_2N$]−Li[$Tf_2N$], $x_{LiTf_2N} = 0.24$, at $T = 25$ °C. The full lines are visual guides.

**Transport Coefficients.** Figure 2 shows density ($\rho$), viscosity ($\eta$), and conductivity ($\sigma$) as functions of $SO_2$ content for neat [BMMI][$Tf_2N$] and [BMMI][$Tf_2N$]−Li[$Tf_2N$] solutions. It is clear that $\rho$ and $\eta$ decrease, whereas $\sigma$ increases, with increasing $x_{SO_2}$. The dissolved $SO_2$ can affect the conductivity of the IL in different ways. Density decreases with $x_{SO_2}$, which implies a smaller number of charge carriers per unit volume; $\sigma$, however, increases with the amount of $SO_2$. The dissolution of $SO_2$ reduces the IL viscosity, which increases the conductivity due to the enhanced ionic mobility. However, Figure 3 shows that the enhancement of conductivity with $SO_2$ content, rather than being simply proportional, is actually larger than the reduction in viscosity. Thus, even though the Raman spectra indicated relatively weak $SO_2$−[$Tf_2N$] interactions in comparison with previous results concerning $SO_2$−$Br^-$ interactions, such interactions with $SO_2$ molecules are still able to reduce the degree of ionic association for both the neat [BMMI][$Tf_2N$] and the [BMMI][$Tf_2N$]−Li[$Tf_2N$] solutions.

The PGSE-NMR method allows the individual determination of the diffusivity of species[31−34] where $^{19}F$, $^1H$, and $^7Li$ nuclei have been used to measure the diffusion coefficient, $D$, of [$Tf_2N$], [BMMI], and $Li^+$, respectively. This measurement does not depend on whether [$Tf_2N$], [BMMI], and $Li^+$ are dissociated, paired species or noncharged aggregates because the rate of exchange for the chemical equilibrium between charged and noncharged species is faster than the time scale of NMR measurements. The dependence of $D$ on $x_{SO_2}$ is shown in Figure 4, where it is clear that $D$ for all ions increases with the

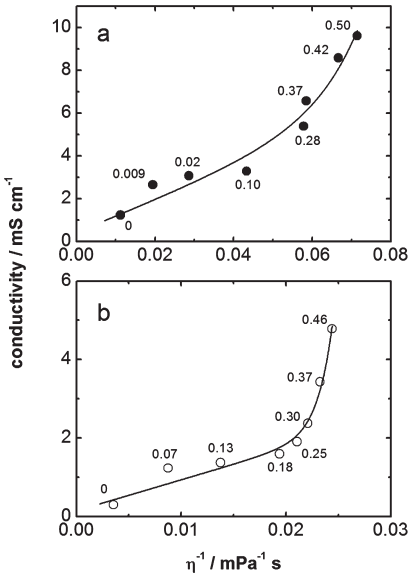


**Figure 3.** Walden plot for different $SO_2$ molar fractions (indicated in the figures) at $T$ = 25 °C: (a) pure [BMMI][$Tf_2N$], and (b) [BMMI][$Tf_2N$]−Li[$Tf_2N$] solution, $x_{LiTf_2N}$ = 0.24. The full lines are visual guides.

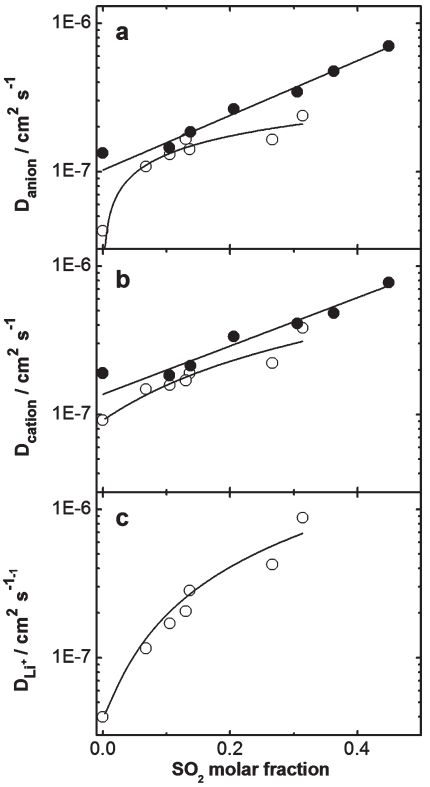


**Figure 4.** Self-diffusion coefficients of (a) [$TF_2N$], (b) BMMI, and (c) $Li^+$ as functions of the $SO_2$ molar fraction at $T$ = 25 °C. The symbols stand for (●) a pure [BMMI][$TF_2N$] and (○) a [BMMI][$Tf_2N$]−Li[$Tf_2N$] solution, $x_{LiTf_2N}$ = 0.24. The symbols are larger than the error bars, and the full lines are visual guides.

amount of $SO_2$. Despite the disparity in the van der Waals radii of [BMMI] (0.55 nm)[35] and [$Tf_2N$] (0.362 nm),[32] the [BMMI]

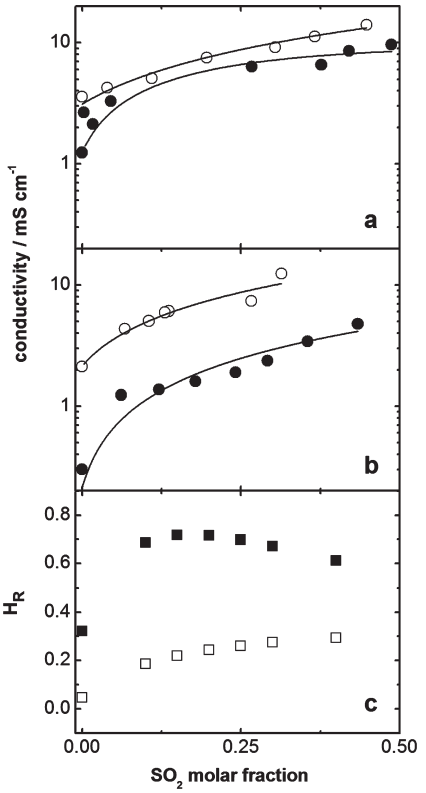


**Figure 5.** Experimental conductivity $\sigma$ (●) and ionic conductivity estimated by eq 3 $\sigma_{NMR}$ (○) as functions of $SO_2$ molar fraction at $T$ = 25 °C. (a) Pure [BMMI][$Tf_2N$], (b) [BMMI][$Tf_2N$]−Li[$Tf_2N$] solution, and (c) the ratio $H_R = \sigma/\sigma_{NMR}$ for (■) pure [BMMI][TFSI], and (□) [BMMI][$Tf_2N$]−Li[$Tf_2N$] solution, $x_{LiTf_2N}$ = 0.24. The full lines are visual guides.

cations diffuse faster than the [$Tf_2N$] in the entire range of $x_{SO_2}$ investigated in this work, which indicates that [$Tf_2N$] does not diffuse as a single species. Normally, $Li^+$ has the smallest diffusion coefficient in ILs[23] despite being the smallest species, which indicates that $Li^+$ forms ionic aggregates. In the case of the [BMMI][$Tf_2N$]−Li[$Tf_2N$] solution, a smaller $D$ is obtained for all ions, even in the presence of $SO_2$; i.e., the interaction between $SO_2$ and ions is not strong enough to avoid the formation of aggregates between [BMMI], [$Tf_2N$] and $Li^+$. Nevertheless, when $SO_2$ is added, $D_{Li^+}$ reaches similar values as $D_{BMMI}$ and $D_{Tf_2N}$. This finding reveals that $SO_2$ is at least able to modify these ionic aggregates.

The relationship between $D$ and $\sigma$ will be discussed by estimating ionic conductivity with the Nernst−Einstein equation, $\sigma_{NMR}$

$$\sigma_{NMR} = \frac{e^2}{kT}\left(n_{BMMI}D_{BMMI} + n_{Tf_2N}D_{Tf_2N} + n_{Li^+}D_{Li^+}\right) \quad (3)$$

where $n_i$ is the number of ions of species $i$ per specific volume, and $e$ is the electron charge. Figure 5 shows that $\sigma_{NMR} > \sigma$ for all values of $x_{SO_2}$, although this difference is smaller for the neat [BMMI][$Tf_2N$] than for the [BMMI][$Tf_2N$]−Li[$Tf_2N$] solution. The ratio $H_R = \sigma/\sigma_{NMR}$ shown in Figure 5c indicates ionic dissociation/association and provides insight into the actual ions contributing to the ionic conductivity. If all the mobile charge carriers were available for conduction, $H_R$ would be equal to 1, whereas $H_R$ < 1 indicates that some of the mobile species


dx.doi.org/10.1021/jp204604r |J. Phys. Chem. B 2011, 115, 9662–9670

**Table 1. Diffusion Coefficient, $D$, Ionic Conductivity, $\sigma_{MD}$, Viscosity, $\eta_{MD}$, and Density Calculated by MD Simulations of [BMMI][$Tf_2N$]−$SO_2$ Solutions at 330 K[a]**

| $x_{SO_2}$ | $D_{BMMI}$ ($10^{-8}$ cm$^2$·s$^{-1}$) | $D_{Tf_2N}$ ($10^{-8}$ cm$^2$·s$^{-1}$) | $\sigma_{MD}$ (mS·cm$^{-1}$) | $\eta_{MD}$ (cP) | density (g·cm$^{-3}$) |
|---|---|---|---|---|---|
| 0.50 | 4.60 | 3.60 | 0.727 | 123 | 1.386 |
| 0.33 | 3.20 | 2.90 | 0.236 | 176 | 1.397 |
| 0.20 | 0.55 | 0.30 | 0.0662 | 360 | 1.399 |
| 0.09 | 0.50 | 0.27 | 0.0739 | 4100 | 1.404 |
| 0 | 0.03 | 0.04 | 0.00732 | – | 1.409 |

[a] The results for $x_{SO_2}$ = 0 correspond to pure [BMMI][$Tf_2N$] at 330 K.

detected in the PGSE-NMR experiment are not contributing to the conductivity. Adding $SO_2$ increases $H_R$, but the effect seems more significant in the case of the neat [BMMI][$Tf_2N$] than in the [BMMI][$Tf_2N$]−Li[$Tf_2N$] solution. Strong [$Tf_2N$]−$Li^+$ interaction is likely the main reason for low $H_R$ in [BMMI][$Tf_2N$]−Li[$Tf_2N$]. Nevertheless, $SO_2$ decreases the interactions among the ions, leaving a greater number of charged species and leading to higher $H_R$ values. Therefore, the larger $H_R$ value in the presence of $SO_2$ also indicates that the increase in conductivity is not solely due to higher fluidity but also to the reduction of ionic aggregates and to the increase in the number of charge-transport species upon addition of $SO_2$.

**Molecular Dynamics Simulations.** The microscopic origin for the increase in $H_R$ with increasing $SO_2$ molar fraction is not completely clear from the above results, because different phenomena could explain the improvement in transport properties by $SO_2$ addition. In a previous MD investigation of [BMMI][$Tf_2N$]−Li[$Tf_2N$], $Tf_2N$ anions have been shown to tightly coordinate $Li^+$ by, forming aggregates that $BMMI^+$ cations are not able to break.[23] With respect to [BMMI][$Tf_2N$]−Li[$Tf_2N$]−$SO_2$ solutions, in which $SO_2$ is the weakest Lewis acid, the competition for the anion is even easier for $Li^+$. Therefore, to understand the role played by $SO_2$ in fluidity, it is sufficient to investigate by MD simulations the [BMMI][$Tf_2N$]−$SO_2$ solutions without lithium cations. As we shall demonstrate in the following sections, the fluidizing effect upon addition of $SO_2$ is due to the competition for $Tf_2N$ between $BMMI^+$ and $SO_2$.

Transport coefficients of [BMMI][$Tf_2N$]−$SO_2$ have been calculated by MD simulations as in previous works.[22,23] Conductivity and diffusion coefficients were calculated by the linear regime of the collective and single particle, respectively, mean square displacement of the ions. Viscosity was calculated by the nondiagonal components of the stress correlation function. Experimentally, the addition of $SO_2$ in [BMMI][$Tf_2N$] changed the transport properties toward a more fluid condensed phase. The results obtained by MD simulations are provided in Table 1 and show the same dependence as the $SO_2$ experiments. It is worth noting that a small amount of $SO_2$ in [BMMI][$Tf_2N$] induces a remarkable change in the calculated transport properties, in line with the experimental data discussed in the previous section. Pure [BMMI][$Tf_2N$] simulated at 330 K seems to be in a glassy state because calculated dynamical properties are 2 orders of magnitude smaller than their respective experimental properties. In fact, nonpolarizable models for ILs are usually too stiff.[36−40] Nevertheless, this important finding from MD simulations represents the correct trend in transport coefficients with $SO_2$ content, even though the absolute values of individual properties might be different from those obtained by experiment. Thus, the major goal of the MD simulations in this work is to elucidate the interplay between dynamical properties and structure.

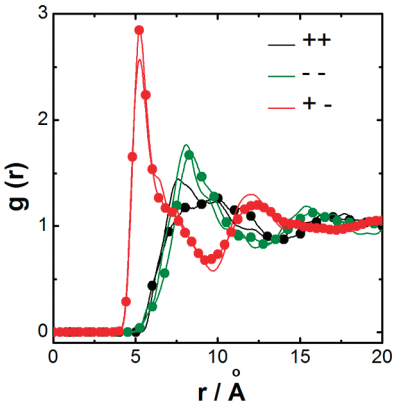


**Figure 6.** Radial distribution functions of the ionic center of mass calculated by MD simulations of pure [BMMI][$Tf_2N$] (full lines) and [BMMI][$Tf_2N$]−$SO_2$ solutions, $x_{SO_2}$ = 0.5 (full circles), at 330 K.

A common feature of simple molten salts and room-temperature ionic liquids is the organization of their microscopic structures by charge ordering. The microscopic structures are characterized by the out-of-phase oscillation of the partial cation−anion radial distribution function, $g_{+-}(r)$, with respect to $g_{++}(r)$ and $g_{--}(r)$. Figure 6 illustrates the charge ordering in neat [BMMI][$Tf_2N$] and [BMMI][$Tf_2N$]−$SO_2$ solutions. The first peak of $g_{--}(r)$ is slightly shifted to larger distances; the peak at 5.3 Å in $g_{+-}(r)$ is not displaced, but its intensity increases upon addition of $SO_2$. The $g_{++}(r)$ is most strongly affected; it becomes broader and the intensity of the short-distance peak at 7.6 Å decreases in the $SO_2$ solution.

Figure 7 shows that the correlation of the $SO_2$ center of mass with the center of mass of [$Tf_2N$] is a shorter distance than with [BMMI]. This result is expected because the $SO_2$ molecule behaves as a Lewis acid and interacts preferentially with the electron-rich species. Figure 8 depicts some partial $g_{\alpha\beta}(r)$ functions, where $\alpha$ and $\beta$ are specific atoms of different species. We have shown in a previous report[23] that the oxygen atoms of [$Tf_2N$] point toward [BMMI], and the correlation between the carbon atoms of the imidazolium ring with oxygen atoms is weakened upon addition of Li[$Tf_2N$]. Unlike a $Li^+$ solution in [BMMI][$Tf_2N$], Figure 8 shows that adding $SO_2$ in [BMMI][$Tf_2N$] does not affect the correlations between the cation C3 atom (the carbon atom between the nitrogen atoms of imidazolium), with O, F, and N atoms of the anion, as anticipated based on the $g_{+-}(r)$ in Figure 6. In fact, this confirms that $Li^+$ is a stronger Lewis acid than $SO_2$ and suggests that $SO_2$ absorbed in [BMMI][$Tf_2N$] causes subtle changes in the local structure of the ionic liquid.

Correlations between $SO_2$ and [$Tf_2N$] are shown in Figure 9. The interaction of $SO_2$ with an anion is more likely between the sulfur atom of $SO_2$ and the oxygen or fluorine atoms of [$Tf_2N$], which are also involved in the interaction with [BMMI]. The first peak of $g_{SF}(r)$ at 3.53 Å is slightly more intense than the peak at 3.49 Å of $g_{SO}(r)$, which means that the $SO_2$ molecule interacts with [$Tf_2N$] by the available atoms that are not participating in the stronger [BMMI]−[$Tf_2N$] interaction. Given the large number of possible atom−atom correlations, the analysis of the local structure of ionic liquids is usually performed by probability

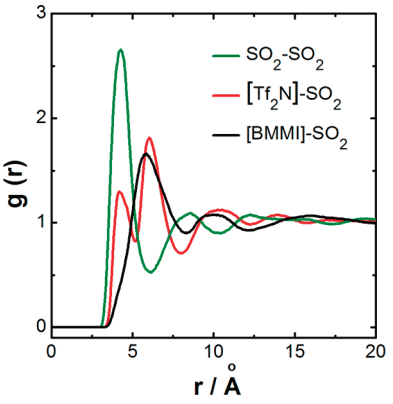


**Figure 7.** Radial distribution functions for the center of mass of $SO_2$ with [BMMI], [$Tf_2N$], and $SO_2$ calculated by MD simulations of [BMMI][$Tf_2N$]−$SO_2$, $x_{SO_2}$ = 0.5, at 330 K.

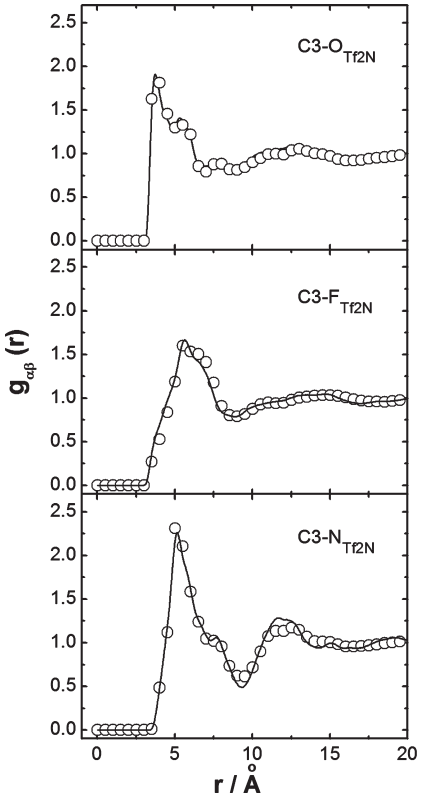


**Figure 8.** Partial $g_{\alpha\beta}(r)$ for the C3 atom (the carbon atom between the nitrogen atoms of imidazolium) of [BMMI] and the atoms of [$Tf_2N$], calculated by MD simulation of pure [BMMI][$Tf_2N$] (full line) and [BMMI][$Tf_2N$]−$SO_2$ solution (open circles), $x_{SO_2}$ = 0.5, at 330 K.

density maps of anions around cations.[41] Figure 10 depicts the probability density map of [$Tf_2N$] and $SO_2$ around [BMMI]. At a low $SO_2$ concentration, the anions are mainly located above and below the imidazolium planar ring (red-colored region). This situation remains intact at higher $SO_2$ concentrations, but the anions shift toward the imidazolium $CH_3$ group. The $SO_2$ molecules are preferentially arranged close to the anions. It should be noted that two regions of $SO_2$ population arise (yellow), with one of them being dispersed in the neighborhood of the nonpolar alkyl chain.

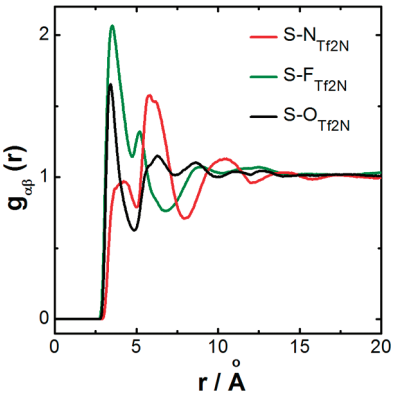


**Figure 9.** Partial $g_{\alpha\beta}(r)$ for the S atom of $SO_2$ and the atoms of [$Tf_2N$], calculated by MD simulation of [BMMI][$Tf_2N$]−$SO_2$, $x_{SO_2}$ = 0.5, at 330 K.

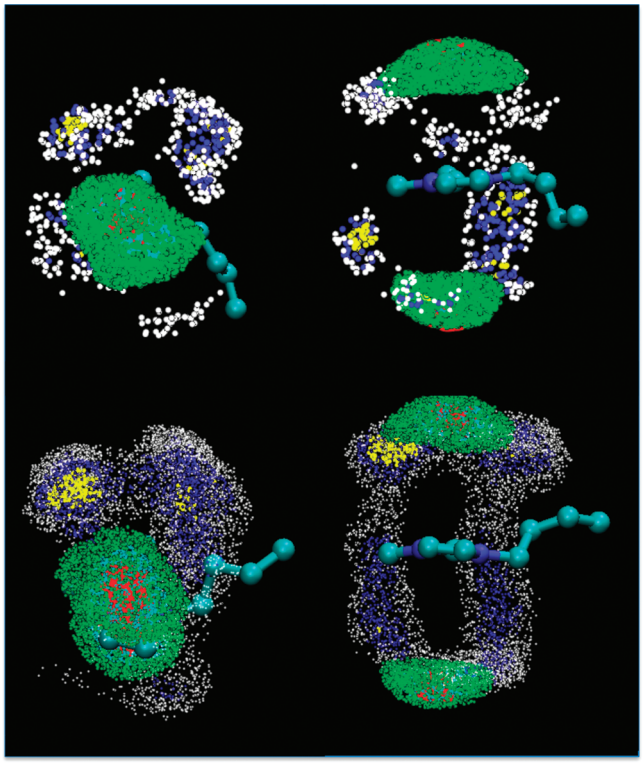

**Figure 10.** Probability density maps of the nearest-neighbor species around [BMMI], as calculated by MD simulations of [BMMI]-[$Tf_2N$]−$SO_2$ solutions. The top figures correspond to $x_{SO_2}$ = 0.09, and the bottom figures to $x_{SO_2}$ = 0.5, in which the left and right figures are two different perspectives. The green and red colors stand for the increasing probability of [$Tf_2N$] anions, whereas the gray, blue, and yellow colors stand for the increasing probability of $SO_2$ molecules within a sphere of radius 6.0 Å around a given [BMMI].

In previous MD simulations of [BMI][Br],[21,22] the drastic changes in physicochemical properties arose from a disruption of the long-range structure of the IL. Stronger local cation−anion pairs occur when $SO_2$ molecules substitute some neighboring ionic species, but the structural order at the non-nearest-neighbor distance is reduced. This explains the simultaneous finding of a high $H_R$ (shown in Figure 5) and a high fluidity of the $SO_2$

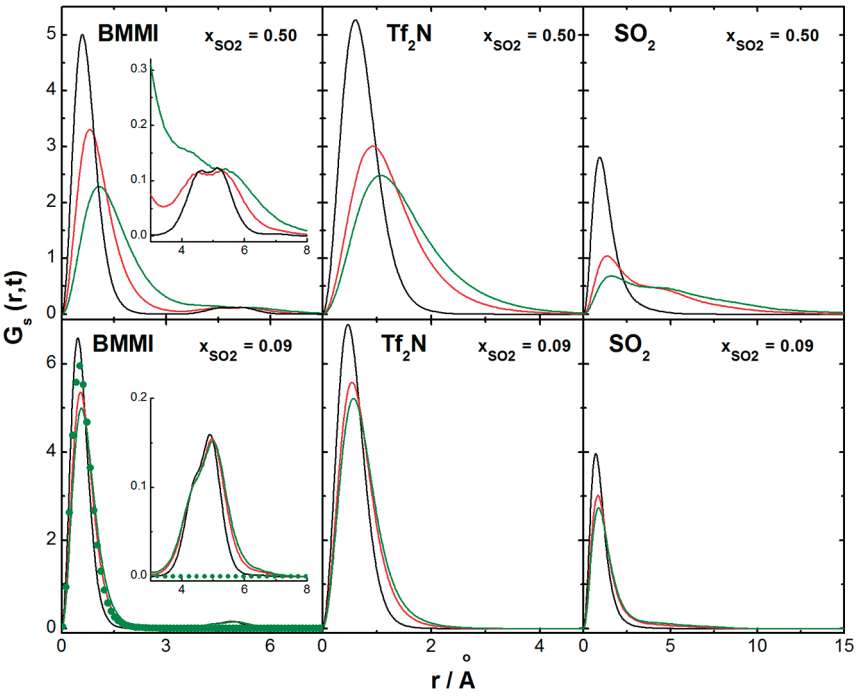


**Figure 11.** Self-part of the van Hove correlation function calculated for [BMMI] (left), [$Tf_2N$] (middle), and $SO_2$ (right) in [BMMI][$Tf_2N$]−$SO_2$ solutions at 330 K and $x_{SO_2}$ = 0.50 and $x_{SO_2}$ = 0.09, at different times: 0.05 ns (black line), 2.0 ns (red line), and 4.0 ns (green line). Insets highlight weak peaks around 5.0 Å. Circles in the left-bottom inset represent $G_s(r,t)$ for cations in pure [BMMI][$Tf_2N$].

solutions in ILs. The relatively strong interaction between $SO_2$ and $Br^-$ was indicated by Raman spectroscopy as a shift to a lower wavenumber of the stretching mode of $SO_2$, $\nu_{SO_2}$.[21] Conversely, in this work, the position of the $\nu_{SO_2}$ Raman band was not affected when $SO_2$ was absorbed by [BMMI][$Tf_2N$] (see Figure 1). However, the transport properties are $SO_2$-dependent in both the experiment and the calculated properties of [BMMI][$Tf_2N$]. Therefore, the structural analysis given above indicates that the microscopic origin of increasing fluidity in [BMMI][$Tf_2N$] due to the addition of $SO_2$ is similar to the previous finding for [BMI][Br].[21,22] In other words, the effect of $SO_2$ in a bromide- or [$Tf_2N$]-based IL is qualitatively analogous, even though the $SO_2$ interaction with [$Tf_2N$] might be weaker than that of bromide. In the following sections, we provide further details on the microscopic dynamics of simulated [BMMI][$Tf_2N$]−$SO_2$ solutions by the calculation of correlation functions that are simultaneously spatially and temporally dependent.

Figure 11 shows the self-part of the van Hove correlation function, $G_s(r,t) = \langle|\mathbf{r}_i(t) - \mathbf{r}_i(0)|^2\rangle$, for the centers of mass of $SO_2$, [$Tf_2N$], and [BMMI] at three different times. The main peak of $G_s(r,t)$ accounts for the displacement of the majority of the species; the cations are relatively slow because the peak takes a longer time to cover a short distance. However, broad and weak peaks appear at approximately 5 Å, which accounts for some [BMMI] (see inset of Figure 11) and $SO_2$ molecules that are relatively fast. These peaks characterize the hopping process for [BMMI] and $SO_2$, but are absent for anions. Notably, [BMMI] cations do not show any evidence of hopping at 330 K in neat [BMMI][$Tf_2N$] (circles in the left bottom inset of Figure 11), which suggests that the fast surrounding $SO_2$ molecules might determine the cations' dynamics.

With regard to the mean square displacement of cations, those cations that have large displacements have been selected and

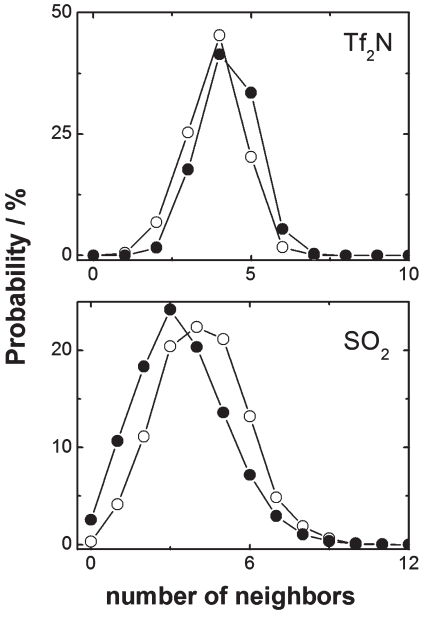


**Figure 12.** Histograms of the number of nearest-neighbor species around fast (open circles) and slow (full circles) [BMMI] cations in [BMMI][$Tf_2N$]−$SO_2$ solutions, $x_{SO_2}$ = 0.50. The top panel shows the histograms of [$Tf_2N$], and the bottom panel shows the histograms of $SO_2$.

labeled as fast cations. These fast cations represent 8−10% of all cations, and they remain fast for a period of time on the order of 1.5 ns. After the fast cations were selected, the number of nearest-neighbor anions and $SO_2$ molecules around them was compared with the majority of nonselected cations. Figure 12 shows

histograms of the probability of finding $[Tf_2N]$ and $SO_2$ inside a sphere of radius 8.0 Å from the center of mass of the fast and "normal" (slow) cations. Although the most probable number of slow and fast cations nearest the anions is similar, the probability of finding slow cations surrounded by five and six $[Tf_2N]$ molecules is greater. Even more remarkable, the local environment of fast cations is characterized by a larger number of surrounding $SO_2$ molecules with a considerable occurrence of cations with five neighboring $SO_2$ molecules. Therefore, Figures 11 and 12 together illustrate the interplay between the local structure and the mobility of [BMMI] cations in $[BMMI][Tf_2N]-SO_2$ solutions.

## CONCLUSIONS

The dissolution of $SO_2$ promotes significant changes in the transport coefficients of the IL $[BMMI][Tf_2N]$ and the mixture $[BMMI][Tf_2N]-Li[Tf_2N]$. The viscosity ($\eta$) decreases, whereas conductivity ($\sigma$) and diffusion coefficients ($D$) increase upon addition of $SO_2$. These changes are not linear with the $SO_2$ content; instead, a sharp change of transport coefficients at a low $SO_2$ concentration is observed, followed by a more smooth change for $x_{SO_2}$ above 0.1. The increase of $\sigma$ is larger than expected from the reduction in viscosity, which indicates that ionic aggregates are modified when $SO_2$ is added to the ionic liquids. In fact, the ratio between the conductivity estimated from $D$ according to the Nernst−Einstein relation, $\sigma^{NMR}$, and the actual conductivity, $H_R = \sigma^{NMR}/\sigma$, increases with $SO_2$ content. The finding that $H_R$ increases also suggests that more free ionic species are available to charge transport. The effects of $SO_2$ are seen in both the neat $[BMMI][Tf_2N]$ and the $[BMMI][Tf_2N]-Li[Tf_2N]$ solution, even though the IL containing $Li^+$ cations remains more viscous and exhibits a smaller conductivity than the pure $[BMMI][Tf_2N]$. However, the lithium diffusion coefficient, $D_{Li}$, becomes comparable with $D_{BMMI}$ and $D_{Tf_2N}$ at high concentrations of $SO_2$. Raman spectroscopy indicated that the strong $Li^+-[Tf_2N]$ interaction is barely affected by the $SO_2$ molecules, and that the $SO_2-[Tf_2N]$ interaction is weaker than previously found in a bromide-based IL.[21,22] A microscopic picture of the $SO_2$ interactions with [BMMI] and $[Tf_2N]$ has been provided by MD simulations. The closer approach occurs between the $SO_2$ and the anion, in particular the oxygen and the fluorine atoms of the $[Tf_2N]$, whereas the structure of $[Tf_2N]$ around [BMMI] is barely affected by the presence of $SO_2$. In fact, the MD simulations showed the importance of $SO_2$ molecules around [BMMI], because the small fraction of these cations that have been identified as more mobile exhibit a larger number of nearest-neighbor $SO_2$ molecules.

## ASSOCIATED CONTENT

**Supporting Information.** Dependence of Raman spectra on the $SO_2$ molar fraction. This material is available free of charge via the Internet at http://pubs.acs.org.

## ACKNOWLEDGMENT

The authors acknowledge CNPq and FAPESP (09/53199-3 and 08/08670-7) for financial support. M.M. thanks FAPESP for a fellowship (05/58525-5).

## REFERENCES

(1) Welton, T. *Chem. Rev.* **1999**, *99*, 2071–2083.
(2) Wasserscheid, P.; Keim, W. *Angew. Chem., Int. Ed.* **2000**, *39*, 3772–3789.
(3) Plechkova, N. V.; Seddon, K. R. *Chem. Soc. Rev.* **2008**, *37*, 123–150.
(4) Earle, M. J.; Seddon, K. R. *Pure Appl. Chem.* **2000**, *72*, 1391–1398.
(5) Anastas, P. T.; Kirchhoff, M. M. *Acc. Chem. Res.* **2002**, *35*, 686–694.
(6) Wilkes, J. S. *Green Chem.* **2002**, *4*, 73–80.
(7) Sheldon, R. A. *Green Chem.* **2005**, *7*, 267–278.
(8) Blanchard, L. A.; Brennecke, J. F. *Ind. Eng. Chem. Res.* **2001**, *40*, 287–292.
(9) Zhang, S. G.; Zhang, Q. L.; Zhang, Z. C. *Ind. Eng. Chem. Res.* **2004**, *43*, 614–622.
(10) Zhou, Y.; Schattka, J. H.; Antonietti, M. *Nano Lett.* **2004**, *4*, 477–481.
(11) Li, Z. H.; Liu, Z. M.; Zhang, J. L.; Han, B. X.; Du, J. M.; Gao, Y. N.; Jiang, T. *J. Phys. Chem. B* **2005**, *109*, 14445–14448.
(12) Ding, K. L.; Miao, Z. J.; Liu, Z. M.; Zhang, Z. F.; Han, B. X.; An, G. M.; Miao, S. D.; Xie, Y. *J. Am. Chem. Soc.* **2007**, *129*, 6362–6363.
(13) Armand, M.; Endres, F.; MacFarlane, D. R.; Ohno, H.; Scrosati, B. *Nat. Mater.* **2009**, *8*, 621–629.
(14) Krossing, I.; Slattery, J. M.; Daguenet, C.; Dyson, P. J.; Oleinikova, A.; Weingartner, H. *J. Am. Chem. Soc.* **2006**, *128*, 13427–13434.
(15) Weingaertner, H. *Angew. Chem., Int. Ed.* **2008**, *47*, 654–670.
(16) Zahn, S.; Bruns, G.; Thar, J.; Kirchner, B. *Phys. Chem. Chem. Phys.* **2008**, *10*, 6921–6924.
(17) Fumino, K.; Wulf, A.; Ludwig, R. *Angew. Chem., Int. Ed.* **2008**, *47*, 8731–8734.
(18) Lassegues, J. C.; Grondin, J.; Cavagnat, D.; Johansson, P. *J. Phys. Chem. A* **2009**, *113*, 6419–6421.
(19) Lassegues, J. C.; Grondin, J.; Cavagnat, D.; Johansson, P. *J. Phys. Chem. A* **2010**, *114*, 687–688.
(20) Wulf, A.; Fumino, K.; Ludwig, R. *J. Phys. Chem. A* **2010**, *114*, 685–686.
(21) Ando, R. A.; Siqueira, L. J. A.; Bazito, F. C.; Torresi, R. M.; Santos, P. S. *J. Phys. Chem. B* **2007**, *111*, 8717–8719.
(22) Siqueira, L. J. A.; Ando, R. A.; Bazito, F. F. C.; Torresi, R. M.; Santos, P. S.; Ribeiro, M. C. C. *J. Phys. Chem. B* **2008**, *112*, 6430–6435.
(23) Monteiro, M. J.; Bazito, F. F. C.; Siqueira, L. J. A.; Ribeiro, M. C. C.; Torresi, R. M. *J. Phys. Chem. B* **2008**, *112*, 2102–2109.
(24) Bazito, F. F. C.; Kawano, Y.; Torresi, R. M. *Electrochim. Acta* **2007**, *52*, 6427–6437.
(25) Ribeiro, M. C. C. *J. Phys. Chem. B* **2006**, *110*, 8789–8797.
(26) Martinez, J. M.; Martinez, L. *J. Comput. Chem.* **2003**, *24*, 819–825.
(27) Berendsen, H. J. C.; Postma, J. P. M.; Gunsteren, W. F.; DiNola, A.; Haak, J. R. *J. Chem. Phys.* **1984**, *81*, 3684–3690.
(28) Allen, M. P.; Tildesley, D. J. *Computer Simulation of Liquids*; Oxford University Press: Oxford, UK, 1987.
(29) Noack, K.; Schulz, P. S.; Paape, N.; Kiefer, J.; Wasserscheid, P.; Leipertz, A. *Phys. Chem. Chem. Phys.* **2010**, *12*, 14153–14161.
(30) Lassegues, J. C.; Grondin, J.; Aupetit, C.; Johansson, P. *J. Phys. Chem. A* **2009**, *113*, 305–314.
(31) Tokuda, H.; Hayamizu, K.; Ishii, K.; Susan, M. A. B. H.; Watanabe, M. *J. Phys. Chem. B* **2005**, *109*, 6103–6110.
(32) Tokuda, H.; Hayamizu, K.; Ishii, K.; Susan, M. A. B. H.; Watanabe, M. *J. Phys. Chem. B* **2004**, *108*, 16593–16600.
(33) Noda, A.; Hayamizu, K.; Watanabe, M. *J. Phys. Chem. B* **2001**, *105*, 4603–4610.
(34) Umecky, T.; Kanakubo, M.; Ikushima, Y. *Fluid Phase Equilib.* **2005**, *228*, 329–333.
(35) Ue, M.; Murakami, A.; Nakamura, S. *J. Electrochem. Soc.* **2002**, *149*, A1385–A1388.

(36) Siqueira, L. J. A.; Ribeiro, M. C. C. *J. Phys. Chem. B* **2007**, *111*, 11776–11785.
(37) Cadena, C.; Zhao, Q.; Snurr, R. Q.; Maginn, E. J. *J. Phys. Chem. B* **2006**, *110*, 2821–2832.
(38) Tsuzuki, S.; Shinoba, W.; Saito, H.; Mikami, M.; Tokuda, H.; Watanabe, M. *J. Phys. Chem. B* **2009**, *113*, 10641–10649.
(39) Koddermann, T.; Paschek, D.; Ludwig, R. *ChemPhysChem* **2007**, *8*, 2464–2470.
(40) Van-Oanh, N.-T.; Houriez, C.; Rousseau, B. *Phys. Chem. Chem. Phys.* **2010**, *12*, 930–936.
(41) Urahata, S. M.; Ribeiro, M. C. C. *J. Chem. Phys.* **2004**, *120*, 1855–1863.